HHS Public Access

Author manuscript

Cell Rep. Author manuscript; available in PMC 2020 June 25.

Published in final edited form as:

Cell Rep. 2020 June 02; 31(9): 107721. doi:10.1016/j.celrep.2020.107721.

Inactivation of Rho GTPases by *Burkholderia cenocepacia* Induces a WASH-Mediated Actin Polymerization that Delays Phagosome Maturation

Glenn F.W. Walpole[1,2], **Jonathan D. Plumb**[1], **Daniel Chung**[1], **Brandon Tang**[1], **Benoit Boulay**[1], **Douglas G. Osborne**[3], **Joshua T. Piotrowski**[3], **Sergio D. Catz**[4], **Daniel D. Billadeau**[3], **Sergio Grinstein**[1,2,6,*], **Valentin Jaumouillé**[1,5]

[1]Program in Cell Biology, Hospital for Sick Children, Toronto, ON M5G 1X8, Canada

[2]Department of Biochemistry, University of Toronto, Toronto, ON M5S 1A8, Canada

[3]Division of Oncology Research and Schulze Center for Novel Therapeutics, Mayo Clinic College of Medicine, Rochester, MN 55905, USA

[4]Department of Molecular Medicine, The Scripps Research Institute, 10550 North Torrey Pines Road, MB-215, La Jolla, CA 92037, USA

[5]Present address: Cell and Developmental Biology Center, National Heart Lung and Blood Institute, National Institutes of Health, Bethesda, MD 20892, USA

[6]Lead Contact

SUMMARY

Burkholderia cenocepacia is an opportunistic bacterial pathogen that causes severe pulmonary infections in cystic fibrosis and chronic granulomatous disease patients. B. cenocepacia can survive inside infected macrophages within the *B. cenocepacia*-containing vacuole (BcCV) and to elicit a severe inflammatory response. By inactivating the host macrophage Rho GTPases, the bacterial effector TecA causes depolymerization of the cortical actin cytoskeleton. In this study, we find that *B. cenocepacia* induces the formation of large cytosolic F-actin clusters in infected macrophages. Cluster formation requires the nucleation-promoting factor WASH, the Arp2/3 complex, and TecA. Inactivation of Rho GTPases by bacterial toxins is necessary and sufficient to induce the formation of the cytosolic actin clusters. By hijacking WASH and Arp2/3 activity, *B. cenocepacia* disrupts interactions with the endolysosomal system, thereby delaying the maturation of the BcCV.

*Correspondence: sergio.grinstein@sickkids.ca.

AUTHOR CONTRIBUTIONS

G.F.W.W., J.D.P., V.J., D.C., B.T., and B.B. conducted experiments. G.F.W.W. and J.D.P. performed image analyses. G.F.W.W., V.J., and S.G. designed the study. D.G.O., J.T.P., S.D.C., and D.D.B. made and provided reagents. G.F.W.W., V.J., and S.G. wrote the manuscript, with input from all authors.

DECLARATION OF INTERESTS

The authors declare no competing interests.

SUPPLEMENTAL INFORMATION

Supplemental Information can be found online at https://doi.org/10.1016/j.celrep.2020.107721.

In Brief

Despite causing profound inhibition of host cell Rho GTPases, *Burkholderia cenocepacia* induces F-actin polymerization near endomembranes, particularly around phagosomes. Walpole et al. show that WASH, an Arp2/3 activator, is required for this *de novo* F-actin polymerization. The F-actin clusters formed around phagosomes delay their maturation, preventing their fusion with lysosomes.

Graphical Abstract

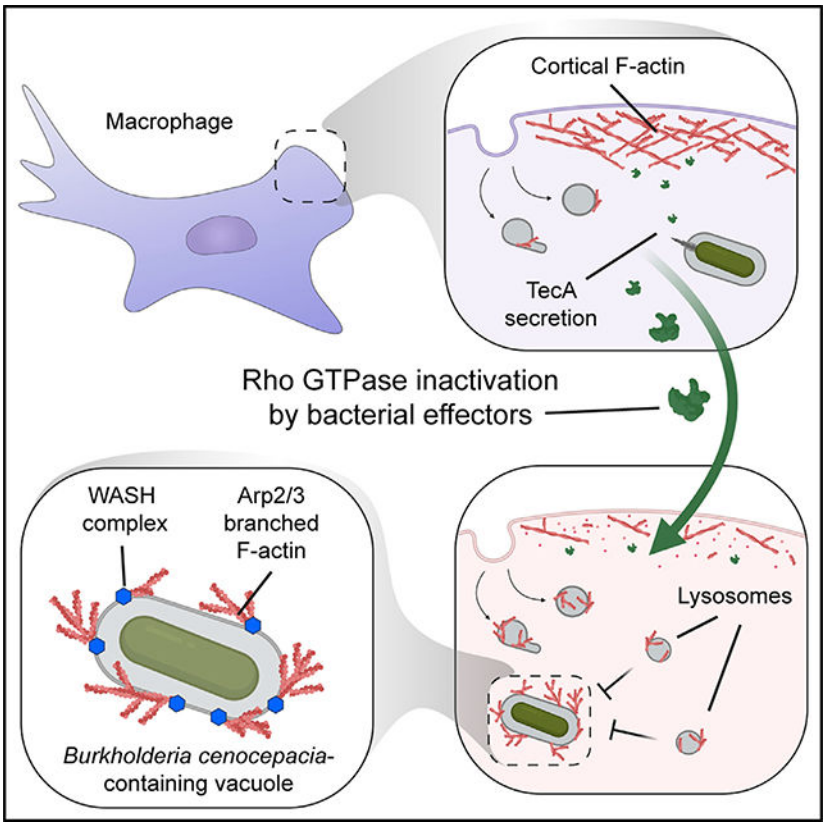

INTRODUCTION

Burkholderia cenocepacia (B. cenocepacia), a Gram-negative bacterium belonging to the *Burkholderia cepacia* complex, emerged in the 1980s as a major opportunistic pathogen for immunocompromised individuals. In the respiratory microbiota of cystic fibrosis patients, *B. cenocepacia* is associated with rapidly progressing necrotizing pneumonia, septicemia, and increased mortality (Isles et al., 1984). This devastating cepacia syndrome is highly transmissible in cystic fibrosis and chronic granulomatous disease patients (Johnston, 2001; Scoffone et al., 2017).

Macrophages in the respiratory tract form a first line of defense against infection. Present both in the mucosa of conducting airways and in alveolar spaces, they ingest and kill foreign organisms and subsequently regulate inflammation (Holt et al., 2008). Remarkably, *B.*

cenocepacia can survive inside macrophages *in vivo* and *in vitro* (Saini et al., 1999; Sajjan et al., 2001). This has been attributed to *B. cenocepacia*'s capacity to divert the host cell intracellular traffic. The *B. Cenocepacia*-containing vacuole (BcCV) matures to an early phagosome stage but delays fusion with lysosomes and fails to acidify its lumen. This occurs at least partly because of inactivation and/or failure to acquire the guanosine triphosphatase (GTPase) Rab7, a major regulator of phagosome maturation (Huynh et al., 2010; Lamothe et al., 2007). Although several bacterial factors are known to support intracellular survival (Keith and Valvano, 2007; Maloney and Valvano, 2006), the host machinery that is targeted remains elusive.

In addition to subverting intracellular traffic, *B. cenocepacia* overhauls the host cell actin cytoskeleton. TecA, a type 6 secretion system effector, irreversibly deamidates Rho GTPases, including Rac1 and RhoA (Aubert et al., 2016). As master regulators of actin networks, their inhibition leads to a drastic impairment of phagocytosis and macropinocytosis (Flannagan et al., 2012; Rosales-Reyes et al., 2012). Rho GTPase inactivation by *B. cenocepacia* also contributes to disproportionate inflammation and major downstream respiratory complications. It is indirectly sensed by the pyrin inflammasome, leading to the secretion of interleukin-1β and inflammatory cell infiltration (Xu et al., 2014).

In this study, we analyzed the consequences of inactivating Rho GTPases on *B. cenocepacia* intracellular survival. We found that despite GTPase inactivation, the bacteria induced *de novo* formation of micron-size clusters of filamentous actin (F-actin) in the macrophage cytoplasm. This process depended on WASH, an endosome-associated nucleation-promoting factor (NPF), which activates the Arp2/3 complex. The accumulation of F-actin near the BcCV delayed phagosome maturation by curtailing access to late endosomes/lysosomes, revealing a role for WASH in bacterial pathogenesis.

RESULTS

B. cenocepacia Induces Accumulation of F-actin Puncta in Infected Macrophages

After internalization by phagocytosis, *B. cenocepacia* drastically alters the morphology of the host cell. This phenomenon is induced by the effector TecA that inactivates several Rho GTPases by deamidation, leading to disassembly of the plasma membrane-associated cortical F-actin and rounding up of infected macrophages (Flannagan et al., 2012; Rosales-Reyes et al., 2012). We replicated these findings in bone-marrow-derived macrophages (BMDMs) (Figures 1A and 1B) and in the macrophage cell line RAW264.7 (Figure S1A) infected with the *B. cenocepacia* strain J2315 (Govan et al., 1993). In addition to cortical actin, internalization of *B. cenocepacia* led to the disassembly of podosomes and loss of lamellipodia (arrows, Figure 1A), resulting in a decrease in the total F-actin content (Figures 1A–1C and S1C). Paradoxically, careful examination of phalloidin-stained cells by confocal microscopy revealed the appearance of submicron- to micron-size intracellular F-actin puncta (Figures 1B, 1D, 1E, and S1A; Videos S1 and S2). Although not exclusively, puncta were often visualized proximal to the BcCV and could form a dense network around engulfed bacteria (Figure S1B). F-actin clusters appeared ≈30 min after bacterial internalization and remained visible for at least 6 h. Together, these results indicate that

during the extensive reorganization of the host actin cytoskeleton caused by *B. cenocepacia*, short actin filaments accumulate inside the cells as the cortical F-actin is depleted.

Inhibition of Rho GTPases Is Required and Sufficient to Induce F-actin Puncta in Macrophages

Because intracellular F-actin puncta appeared concomitantly with the disruption of the cortical cytoskeleton, we sought to test the role of Rho GTPases in the process. To this end, we infected macrophages with isogenic wild type (WT) and with *ΔtecA* bacteria and monitored changes to the actin cytoskeleton. Infection of BMDMs and RAW264.7 cells with WT, but not *ΔtecA* bacteria, led to a distinct increase in intracellular F-actin puncta (Figures 1E and 1F). The requirement for TecA was evident: decreased cortical F-actin, cell rounding (Figures 1E and S1C), and decreased total F-actin were observed only in cells infected with WT, but not *ΔtecA* bacteria (Figures 1C and S1C). Surprisingly, deletion of *tecA* not only restored total F-actin levels but also led to a modest increase relative to control cells (Figure 1C) that could be mimicked by incubating cells in lipopolysaccharide (data not shown).

To further analyze the connection between Rho GTPase inactivation and formation of intracellular F-actin puncta, we used toxin B of *Clostridioides difficile* (TcdB). TcdB irreversibly inactivates GTPases of the Rho family, including Rac, Cdc42, and RhoA (Jank and Aktories, 2008). In an infection-free system, TcdB caused prototypical macrophage rounding and decreased total cellular F-actin content (Figure 1H). Importantly, it also induced a marked increase in intracellular F-actin puncta (Figures 1G, 1I, and S1D). Contrary to Rho GTPase inhibition, inhibiting actin polymerization by latrunculin A disassembled the cortical F-actin but failed to phenocopy the accumulation of intracellular F-actin puncta, suggesting that puncta are not cortical breakdown products (Figures S2A and S2B). Instead, the results indicate that inactivation of Rho GTPases is both necessary and sufficient to generate intracellular F-actin clusters in macrophages. F-actin clusters were not as apparent in HeLa cells treated with TcdB (Figure S2C) despite acquiring rounded morphology, suggesting that this phenomenon is more pronounced in some cell types.

F-actin Puncta Are Coupled to WASH-Associated Endosomal Compartments

In cells, actin polymerization is initiated by actin nucleators such as the Arp2/3 complex, which is activated by NPFs (Pollard and Cooper, 2009). We hypothesized that one such NPF could facilitate de novo synthesis of intracellular F-actin clusters during *B. cenocepacia* infection. Wiskott-Aldrich syndrome protein (WASp) and WAVE are predominant NPFs activated by Cdc42 and Rac, respectively (Takenawa and Suetsugu, 2007), but both GTPases are inactivated during *B. cenocepacia* infection (Flannagan et al., 2012), making these NPFs unlikely candidates. An alternative NPF is WASH, which activates Arp2/3 on endosomes to promote cargo sorting and recycling (Seaman et al., 2013; Simonetti and Cullen, 2019; Wang et al., 2018). Endogenous WASH, which forms discrete structures when immunostained in macrophages, was found to be consistently juxtaposed to the F-actin clusters formed following the internalization of *B. cenocepacia* or upon treatment with TcdB (Figures 2A, 2B, and S2D; Videos S3 and S4). Because WASH appeared immediately beside, but not necessarily overlapping, the actin puncta, their association was analyzed using Statistical Object Distance Analysis (SODA) (Lagache et al., 2018). SODA considers

signal geometry and density to determine the probability of molecular associations, rather than strictly assessing colocalization. SODA revealed that the spatial distribution of these two proteins was not random: a high coupling probability exists between WASH and F-actin puncta (maximum coupling probability = 0.795 between 132 to 264 nm, i.e., rings r_2–r_3 in Figures 2C and 2D). The association was highly significant, with $p < 10^5$ up to 528 nm (i.e., rings r_1–r_4) relative to randomly distributed particles.

WASH can be recruited to Rab7-positive endosomes and a transitioning pool of Rab5-positive endosomes via the Retromer complex (Rojas et al., 2008; Seaman et al., 2009). Given the maturation delay of the BcCV, which allows the persistence of intraphagosomal bacteria (Huynh et al., 2010; Keith et al., 2009; Lamothe et al., 2007), we speculated that the accumulation of WASH-associated F-actin might be related to an interference of endosomal traffic. Thus, we assessed whether the intracellular F-actin clusters associate with particular endosomal compartments. As shown in Figures 2E and 2F, F-actin puncta formed after *B. cenocepacia* internalization, associated with endocytic membranes of both early origin (GFP-Rab5 positive, 30.6% of total puncta) and late/lysosome origin (GFP-Rab7 positive, 70.8% of total). Jointly, these observations suggested that F-actin clusters induced by Rho GTPase inactivation were associated with endosomes and that their formation may be mediated by WASH.

WASH Is Required for Formation of F-actin Clusters in Response to Rho GTPase Inactivation

We proceeded to assess the role of WASH in the formation of actin puncta. Because global knockout of *Washc1* (encoding WASH) is embryonic lethal, we used two primary murine macrophage models devoid of WASH: a tamoxifen-inducible knockout generated by estrogen receptor-Cre recombinase (hereafter *Washout*) (Gomez et al., 2012) and a hematopoietic-specific knockout of *Washc1* (hereafter *Washc1*$^{-/-}$) generated by Vavdriven Cre recombinase expression (Graham et al., 2014). WASH deletion was confirmed by immunoblotting (Figures 3A and 3B). Phalloidin staining revealed that the small intracellular F-actin puncta typically observed in uninfected WT BMDMs (which required overexposure for satisfactory illustration), indicative of basal WASH activity on normal endosomes, were absent from Washout and Washc1$^{-/-}$ macrophages (Figures 3C and S3A).

During infection by B. cenocepacia, deletion of WASH did not interfere with bacteria uptake, because a comparable (in fact, slightly higher) number of bacteria were taken up by *Washout* macrophages (Figure S3B). Moreover, internalized bacteria disassembled cortical F-actin, as indicated by cell rounding, regardless of the presence of WASH (Figure 3D). Strikingly, the cytosolic clusters of F-actin normally induced by *B. cenocepacia* were markedly reduced in the absence of WASH (≈70% in Washout BMDMs and more than 90% in *Washc1*$^{-/-}$ BMDMs) (Figures 3D, 3E, and S3C). Cytosolic F-actin clusters were virtually undetectable in infected macrophages (Figure 3D), and only faint diffuse/reticular staining was occasionally seen throughout the cytoplasm (Figure S3D). Similarly, the induction of intracellular F-actin puncta by TcdB required WASH (Figures 3F and 3G). In contrast, intracellular F-actin puncta readily formed in infected WAS$^{-/-}$ BMDMs (Figure S3E). Thus, we concluded that WASH is dispensable for phagocytosis of *B. cenocepacia* but is required

for the accumulation of F-actin clusters in the cytosol of macrophages following inactivation of Rho GTPases.

Formation of Intracellular Actin Puncta Requires Arp2/3-Mediated Nucleation

As a member of the WASp family, WASH is capable of activating Arp2/3 (Derivery et al., 2009). Because cytosolic F-actin puncta were not formed upon latrunculin treatment (Figure S2), we speculated thatRhoGTPaseinactivationinduceddenovoactin polymerization by Arp2/3, recruited to endosomes by WASH. To test this model,weimmunostained endogenous ArpC2,a coreArp2/3 subunit, in BMDMs (Figure 4). ArpC2 was found to juxtapose and partially colocalize with F-actin puncta formed in macrophages infected with *B. cenocepacia* (Figure 4A) or treated with TcdB (Figure 4B). Furthermore, striking enrichment of ArpC2 occurred on the BcCV that coincided with the acquisition of F-actin (Figure S4).

To assess the role of Arp2/3 in the formation of the F-actin puncta formed upon inactivation of Rho GTPases, we used the Arp2/3 inhibitor CK-666 (Nolen et al., 2009). BMDMs were preincubated with TcdB before treatment with vehicle or CK-666 to avoid possible effects of the Arp2/3 inhibitor on TcdB uptake. As shown in Figures 4C and 4D, CK-666 greatly reduced the number of F-actin puncta near WASH, which retained its punctate distribution. In contrast, treatment of BMDMs with the formin inhibitor SMIFH2 (Rizvi et al., 2009) failed to alter the number of F-actin puncta (Figure 4D). These results indicated that formation of intracellular F-actin clusters following Rho GTPase inactivation requires Arp2/3-mediated actin polymerization.

WASH Is Not Required for Pyrin Inflammasome Activation

Inactivation of Rho GTPases by *B. cenocepacia* triggers pyrin inflammasome activation, leading to inflammatory cell infiltration and tissue damage (Xu et al., 2014). Pyrin localizes to F-actinrich structures in resting cells, and a direct interaction of pyrin with actin and Arp3 has been reported (Mansfield et al., 2001; Waite et al., 2009). This raised the possibility that WASH-dependent F-actin puncta accumulation could be involved in pyrin inflammasome activation.

Inflammasome activation is accompanied by the clustering of the adaptor protein ASC and caspase-1 cleavage (Masumoto et al., 1999). As reported (Aubert et al., 2016), exposure of WT BMDMs to B. cenocepacia led to the formation of micron-size ASC foci that were detectable in a fraction of cells and depended on TecA (Figures S5A–S5C). A similar response was elicited in WT and Wash c1$^{-/-}$ BMDMs (Figures S5F and S5G), suggesting that WASH is not required for pyrin inflammasome activation. We validated this conclusionbyanalyzingtheactivationofcaspase-1andensuingpyroptosis of infected cells, which strictly depended on TecA (Figures S5D and S5E). The cleavage of caspase-1 was similarly activated in WT and *Washc1*$^{-/-}$ BMDMs (Figure S5H), confirming that WASH is not essential for pyrin inflammasome activation.

WASH and Arp2/3 Activity Mediate Delayed Phagosome Maturation during *B. cenocepacia* Infection

We next analyzed whether the increase in WASH-mediated actin polymerization had other consequences for the infection process. Internalized by WT BMDMs showed limited (≈25%) colocalization with fluorescent dextran 4 h after infection (Figures 5C–5E). Remarkably, at this time, more than 50% of the vacuoles containing live *B. cenocepacia* internalized by Washout BMDMs were dextran positive (Figures 5D and 5E). The percentage of live B. cenocepacia found in dextran-positive compartments 6 h after infection decreased in the *Washout* BMDMs. This suggests that WASH delays but does not fully impair fusion of the BcCV with ly-Intracellular survival of *B. cenocepacia* has been related to a delay in the fusion of the BcCV withlysosomes (Burns etal., 1996; Huynh et al., 2010; Lamothe et al., 2007). Because WASH is involved in endosomal traffic and sorting, hijacking its activity could potentially affect BcCV maturation. Consistently, internalized live *B. cenocepacia*, but not inactivated bacteria, accumulated F-actin intheimmediatevicinityoftheBcCV in regions devoid of late endosomes/lysosomes marked by LAMP-1 (Figures 5A and 5B).

To test the putative contribution of WASH to BcCV maturation, we compared the rate of lysosomal fusion to the vacuole in WT and *Washout* BMDMs. Lysosomes were loaded with dextran conjugated to tetramethylrhodamine-dextran, a pH-insensitive fluorophore, before infection of BMDMs with live or dead *B. cenocepacia*, and the fusion of dextran-loaded lysosomes with the BcCV was monitored over time. At 80 min post-infection, >70% of BcCV containing dead bacteria had fused with fluorescent dextran in both WT and Washout BMDMs, suggesting that WASH is dispensable for normal phagosome-lysosome fusion (Figures 5C–5E). Dead B. cenocepacia were no longer visible 4 or 6 h after ingestion, indicating that they had been degraded. Similar to a previous report in RAW264.7 cells (Lamothe et al., 2007), vacuoles containing live *B. cenocepacia* sosomes. Instead, this observation may result from the degradation of the subpopulation of bacteria that became exposed to lysosomal enzymes; their disappearance would decrease the denominator, increasing the apparent fraction of viable bacteria (i.e., those residing in dextran-free BcCVs).

We next tested whether the delay in BcCV maturation attributable to WASH is mediated by its ability to activate Arp2/3. RAW264.7 macrophages were treated with vehicle or CK-666 following the internalization of live or dead *B. cenocepacia*. Although the inhibition of Arp2/3 did not affect fusion of lysosomes with BcCVs containing dead bacteria, disrupting Arp2/ 3-mediated actin polymerization increased the fusion of BcCVs containing live *B. cenocepacia* with lysosomes, as indicated by their acquisition of dextran (Figure 5F). Jointly, these observations imply that *B. cenocepacia* hijacks WASH and thereby Arp2/3 activity to delay the maturation of the BcCV.

DISCUSSION

We report that although inactivation of Rho GTPases by *B. cenocepacia* or TcdB induces disassembly of plasmalemma-associated actin, these treatments do not lead to the disassembly of all pools of F-actin. Although the net F-actin content of the cells decreases,

there is concomitant amplification of endosome-associated actin structures that form under the control of WASH (Figure 3) and Arp2/3 (Figure 4). Moreover, we found that this aberrant buildup of endomembrane-associated F-actin has important consequences on the response of macrophages to *B. cenocepacia* infection: WASH-dependent F-actin formation upon Arp2/3 activation contributes to the delay in BcCV maturation (Figure 5).

Disassembly of the Cortical F-actin Network Leads to a WASH- and Arp2/3-Dependent Accumulation of F-actin Clusters

During macrophage infection, B. cenocepacia stimulated the formation of F-actin structures through WASH, an NPF that activates Arp2/3 (Derivery et al., 2009). How TecA, the bacterial effector from *B. cenocepacia*, or TcdB accomplishes this feat is unclear, at least partly because WASH regulation remains incompletely understood. Other NPFs, such as WASp or WAVE, are activated by Rho GTPases (Takenawa and Suetsugu, 2007). However, mammalian RhoA, Rac1, and Cdc42 fail to activate the WASH complex *in vitro* (Jia et al., 2010). On the contrary, our findings imply that inhibition of Rho GTPases suffices to induce WASH- and Arp2/3-dependent actin polymerization. In mammalian cells, WASH activity can be enhanced upon ubiquitination by the E3 ligase TRIM27 (Hao etal., 2015,2013) or following phosphorylation by Btk (Tsarouhas et al., 2019). It is unlikely that these mechanisms are involved here, given that rather different enzymatic activities, GTPase glucosylation by TcdB and deamidation by TecA, mediate an analogous outcome. Instead, we propose that Rho GTPase inactivation may cause stimulation of WASH by making accessible rate-limiting factors that, under normal conditions, are engaged by other Rho GTPase-dependent actin pools.

Competition among actin pools has been demonstrated in other cellular models. For instance, the G-actin-binding protein profilin regulates the balance between Arp2/3 and formin-driven actin filaments, whereas it has little effect on the overall G-actin/ F-actin ratio (Rotty et al., 2015; Suarez et al., 2015). In addition, in the *Drosophila* airway epithelium, formin-mediated apical actin bundles and endosomal actin networks are antagonistically regulated by Btk29A (the ortholog of mammalian Btk) that directly phosphorylates WASH (Tsarouhas et al., 2019). In these systems the availability of actin monomers appears to be the limiting factor that balances the different actin networks: as one network is inhibited or disadvantaged, more actin monomers become available to fuel the other networks (Suarez and Kovar, 2016). Surprisingly, the phosphomimetic-activation of WASH sufficed not only to induce endosomal actin patches but also to reduce apical F-actin bundling, suggesting direct competition between these actin networks (Tsarouhas et al., 2019). In agreement with this model, when macrophages were infected by *B. cenocepacia* or treated with TcdB, the cortical cytoskeleton was drastically disassembled, yet the total F-actin content was only modestly decreased because of the coincident increase of endosomal F-actin (Figure 1). Thus, it is likely that once predominant actin polymerization events were downregulated by the inhibition of the Rho GTPases, actin turnover released monomers that fueled WASH-dependent actin polymerization. Finally, the inactivation of Cdc42 and Rac1 by B. cenocepacia, which is expected to depress the stimulation of WASp and WAVE, would liberate Arp2/3, which may also be a factor limiting the ability of WASH to polymerize actin. Strikingly, in myeloid cells, WASp is expressed at a concentration that is

approximately the same as that for Arp2/3 (Higgs and Pollard, 2000). Consequently, one can envision that increasing the availability of Arp2/3 would favor the expansion of the WASH-associated endosomal actin network.

Hijacking WASH Activity Affects Phagosome Maturation

Phagosome maturation occurs by sequential fusion with early endosomes, late endosomes, and lysosomes. Concomitant fission events remove unwanted components and maintain the vacuolar surface essentially unchanged. Maturation of phagosomes containing viable *B. cenocepacia* is delayed by a mechanism that is not well understood. The present study suggests that WASH plays a role in the maturation delay (Figure 5), which was reported to reduce the rate of acidification and the delivery of microbicidal hydrolases, favoring bacterial survival in the phagosome (Huynh et al., 2010; Lamothe et al., 2007).

How could WASH be involved in altering the fate of the BcCV? In uninfected cells, WASH is recruited to endosomes through multiple molecular complexes including the Retromer (Rojas et al., 2008; Seaman et al., 2009), the ESCRT-0 component HRS (MacDonald et al., 2018), and possibly direct lipid interactions (Derivery et al., 2009; Jia et al., 2012). Conversely, the WASH complex is required for the association of the CCC and Retriever recycling complexes with endosomes (McNally et al., 2017; Phillips-Krawczak et al., 2015). Together with sorting nexin proteins, the WASH complex functions as a master regulator for sorting and recycling cargo proteins out of the endocytic pathway (Simonetti and Cullen, 2019; Wang et al., 2018). Though not fully understood, WASH is responsible for the formation of actin patches on the surface of endosomes, which may constrain cargo into discrete sites for recycling (Puthenveedu et al., 2010) and promote scission of recycling vesicles (Derivery et al., 2009). Conceivably, the diversion of WASH may impair the ability of phagosomes to undergo proper cargo sorting and scission, thereby affecting the timing of the maturation sequence. This could explain why BcCV simultaneously display markers of compartments that are normally well separated and discrete in uninfected cells (Sajjan et al., 2006). Aberrant WASH-mediated actin polymerization has also been described in cells lacking VAP-A and VAP-B (Dong et al., 2016). These endoplasmic reticulum (ER)-anchored membrane proteins intimately contact multiple cellular organelles, including endosomes, to facilitate the exchange of lipids between bilayers. WASH-positive endosomes can associate with the ER through an interaction of Sorting nexin 2 and VAP-B (Dong et al., 2016). Given the association of ERmarkers with the BcCV (Sajjan et al., 2006), aberrant phagosome-ER contacts may occur in the presence of live B. cenocepacia. Finally, the excessive accumulation of F-actin near the BcCV could create a physical barrier that impedes vesicle fusion, as does the actin cortex during exocytosis or virus release (Arakawa et al., 2007; Villanueva et al., 2012).

In summary, our data revealed a link between regulation of the endosomal actin cytoskeleton and Rho GTPase activities. The inactivation of Rho GTPases by B. cenocepacia TecA or TcdB led to unexpected accumulation of endomembrane-associated actin at the expense of cortical actin. This required WASH and Arp2/3 and induced delayed maturation of the BcCV. The relationship of events occurring locally at the surface of the phagosome

containing live and dead prey, particularly the regulation of the local actin assembly and its effects on maturation, remains incompletely understood and warrants further investigation.

STAR+METHODS

RESOURCE AVAILABILITY

Lead Contact—Further information and requests for resources and reagents should be directed to and will be fulfilled by the lead contact, Sergio Grinstein (sergio.grinstein@sickkids.ca).

Materials Availability—This study did not generate new unique reagents.

Data and Code Availability—This study did not generate any unique datasets or code.

EXPERIMENTAL MODEL AND SUBJECT DETAILS

Cell isolation—Primary murine bone marrow-derived macrophages (BMDM) were prepared from the femurs and tibias of 10–20-week old C57BL/6 wild-type or Washc1$^{flox/flox}$ mice in conjunction with *Washc1*$^{flox/flox}$/ER-Cre^{+} mice (Gomez et al., 2012), *Vav1-Cre*$^{+}$/*Washc1*$^{flox/flox}$ mice (Graham et al., 2014), or WAS$^{-/-}$ mice (Zhang et al., 1999); male and female mice were used indistinctly, with similar results. Euthanized mice were dissected, and cleaned bones were immersed in 70% ethanol for 5 min, dried, and their ends cut off. Bone marrow was centrifuged (15,000 × g, 10 s) into cold PBS, washed once in sterile distilled water to lyse red cells, and pelleted in cold PBS (500 × g, 10 min). Pellets were suspended in BMDM medium (DMEM with 10% FBS, 10 ng/mL M-CSF, 1× antibiotic-antimycotic solution) and plated at a density of 4.0×10^5 cells per 10 cm untreated Petri dish for 5–8 days. In the *Washc1*$^{flox/flox}$/ER-Cre^{+} model, the second exon of the *Washc1* gene was flanked by *lox*P sites, and the expression of an estrogen receptor-Cre recombinase fusion enabled site-specific *Washc1* deletion upon addition of tamoxifen. 100 nM (Z)-4-Hydroxytamoxifen was added to BMDM medium from day 3 until day 7 or day 8 when experiments were completed. *Washc1*$^{flox/flox}$/ER-Cre^{+} BMDM were called Washout and *Washc1*$^{flox/flox}$ BMDM were called *Wash*$^{+/+}$ after treatment with (Z)-4-Hydroxytamoxifen. BMDM from *Vav1-Cre*$^{+}$/*Washc1*$^{flox/flox}$ animals are referred to as *Washc1*$^{-/-}$ throughout.

Cell cultures—RAW264.7 monocyte macrophages (male) were cultured in DMEM supplemented with 10% FBS without antibiotics and were split by scraping every 2–3 days. HeLa cells (female) were cultured in DMEM supplemented with 10% FBS without antibiotics and were split by trypsinization every 4–5 days. All cell types were maintained at 37C in 5% CO_2 incubators. Cells were screened for mycoplasma contamination with Hoechst or DAPI staining and were not propagated past passage 25.

Bacterial cultures—A detailed list of strains utilized in this study is provided in the Key Resources Table. Burkholderia cenocepacia was grown overnight in LB medium with agitation at 37C in the presence of 100 mg/mL carbenicillin (WT J2315, DtecA J2315) or 100 mg/mL trimethoprim (WT J2315 pJRL1). On the day of infection, strains were sub-

cultured to OD_{600} of 0.2 in fresh LB medium without antibiotics and grown with agitation at 37C to OD_{600} of 0.8 at which point 1.0×10^8 bacteria were pelleted and utilized for downstream analyses.

METHOD DETAILS

Macrophage Infection—Between 5 and 8 days after plating BMDM on untreated Petri dishes, cells were rinsed with warm PBS, dissociated with 5 mM EDTA, counted, and seeded on glass coverslips in 12-well plates the day prior to experiments. BMDM were seeded at 5×10^5 cells per well to analyze caspase-1 activation and 3.5×10^5 cells per coverslip for all other experiments. RAW264.7 monocyte macrophages were seeded on coverslips in 12-well plates at a density of 1×10^5 cells one day prior to infection or 5×10^4 cells two days prior to infection for transfection.

Following sub-culture of *B. cenocepacia* in fresh LB medium without antibiotics, 1.0×10^8 bacteria were pelleted (14,000 × g, 2 min) and resuspended in PBS. Unopsonized bacteria were diluted directly into serum-free DMEM for infection or, alternatively, bacteria were opsonized in 200 mL of sterilized human serum for 15 min shaking (500 rpm) at 37C prior to dilution in serum-free DMEM. Opsonized bacteria were re-suspended vigorously to break apart agglutinated bacteria. To fluorescently label bacteria prior to infection, 1.0×10^8 bacteria were shaken (500 rpm) in PBS pH 7.4 containing 25 mg/mL N-hydroxysuccinimide (NHS) ester for 15 min at 37C. Fluorescently-labeled bacteria were washed twice in PBS prior to opsonizing with human serum. To generate intact, dead bacteria for infection, wild-type J2315 were fixed in 8% PFA rotating for 30 minutes. Bacteria were washed with PBS multiple times prior to dilution in serum-free DMEM.

The internalization of bacteria was synchronized by bathing macrophages in serum-free DMEM containing bacteria diluted to the appropriate multiplicity of infection (MOI; generally between 10 and 20 and described individually within each Figure Legend), followed by centrifugation (200 × g, 1 min). Cells were returned to 37C in a humidified 5% CO_2 incubator for 20 min, washed with PBS, and serum-free DMEM was replaced for the remainder of the experiment.

Transfection—RAW264.7 cells were transfected in complete medium z14–18 hours prior to infection using FuGENE HD. Briefly, 0.5 mg of plasmid DNA was combined with FuGENE HD in serum-free DMEM at a 3:1 ratio (μL FuGENE HD: μg cDNA), incubated for 15 min, and added dropwise to 5×10^4 cells seeded the day prior to transfection.

Immunofluorescence—At the indicated times, cells were fixed in 2% PFA for 20 min at room temperature and washed twice with PBS. For LAMP-1 immunostaining, cells were permeabilized for 30 min with 0.2% saponin in PBS supplemented with 10% goat serum (SS-PBS). Primary and secondary antibodies diluted in SS-PBS were overlaid consecutively on coverslips for 60 min, separated by PBS washes.

For all other immunostaining and phalloidin staining, cells were permeabilized by treating with 0.1% Triton X-100 for 5 min, washed twice with PBS, and blocked with 2% BSA in

PBS for 15 min. Primary and secondary antibodies were each overlaid for 60 min in 1% BSA, separated by PBS washes.

Reagents—As specified in Figure Legends, *C. difficile* toxin B (TcdB) was diluted to 100–150 ng/mL in serum-free DMEM and incubated with BMDM or RAW264.7 macrophages. Following a 20-min pre-incubation with TcdB, DMSO (vehicle), Arp2/3 inhibitor CK-666 (50 mM), or formin homology 2 domain inhibitor SMIFH2 (5 mM) was added for the duration of the experiment. Alternatively, DMSO or CK-666 was added following the 20-min uptake of *B. cenocepacia*. RAW264.7 macrophages were treated with 1 μM Latrunculin A for up to 20 min, as indicated in the Figure.

Antibodies were diluted as follows for immunostaining: mouse anti-ASC (1:100), rat anti-LAMP-1 (1:100), rabbit anti-p34-Arc/ARPC2 (1:200), and rabbit anti-WASH (1:1000). All secondary antibodies were diluted at 1:500. Alexa Fluor 488 phalloidin was diluted 1:250 before adding to cells for 1 hour. 5 mg/mL DAPI was diluted 1:3000 in PBS before incubating cells for 12 min and washing thoroughly with PBS. For western blotting, antibodies were diluted and incubated as follows: rabbit anti-caspase-1 (1:400, overnight 4C), rabbit anti-WASH (1:2000, overnight 4C), mouse anti-GAPDH (1:2500, 1.5 hr room temperature).

Lysosome Loading with Fluorescent Dextran—Lysosome loading with dextran by pulse-chase was performed by the method previously established (Johnson et al., 2016). Briefly, BMDM or RAW264.7 macrophages were incubated with 0.1 mg/mL of Alexa Fluor 647-conjugated 10,000 MW dextran, overnight in culture medium. Cells were then washed 3 times with dextran-free medium and incubated for 2 hr to allow full transfer of the fluorescent dextran to lysosomes prior to infection.

Inflammasome Assays—LPS-primed (250 ng/mL) BMDM were treated for 30 min with nigericin sodium salt (20 mM in ethanol) to activate the NLRP3 inflammasome as a positive control for all assays. Control cells were left unprimed.

Cytotoxicity was determined by assaying the percentage of LDH released into serum-free DMEM using the following formula:

$$\%\ LDH\ Release = \frac{(Experimental - Medium)}{(Lysis - Lysis\ Medium)} \times 100$$

Lysis was determined from control cells treated with Triton X-100, Lysis Medium is DMEM containing Triton X-100, and Medium is the absorbance of blank DMEM. All conditions were analyzed in triplicate according to the manufacturers protocol.

Caspase-1 activation was assessed by precipitating cell supernatants in 15% trichloroacetic acid (TCA) solution on ice for > 60 min. TCA was diluted into ddH_2O immediately prior to use. Precipitated supernatants were centrifuged at 14,000 × g, 4C for 15 min, supernatants were carefully removed, and pellets were washed twice with ice-cold acetone to remove residual acid. Air-dried pellets were resuspended in 2× Laemmli-buffer, boiled, and re-

combined with cell lysates prior to western blotting. Samples were resolved on a 15% Tris-glycine gel by SDS-PAGE and transferred onto polyvinylidene fluoride (PVDF) for 35 minutes at 100 V on ice to visualize the 10 kDa p10 subunit. All other western blots were performed by resolving samples on a 10% Tris-Glycine gel by SDS-PAGE and transferring onto PVDF for 60 min at 100 V.

Spinning disk confocal and Lightning microscopy

Spinning disk confocal imaging was performed with a Quorum spinning disk confocal head on a Zeiss Axiovert 200M microscope, equipped with a 63× NA 1.4 oil objective and 25× NA 0.8 multi-immersion objective, a 1.5× tube lens, and a back-thinned EM-CCD camera (C9100–13, Hamamatsu). Acquisition settings were controlled using Volocity software and were acquired at equal laser and exposure settings within experiments across compared conditions. Lightning microscopy was performed on a Leica SP8 Lightning Confocal DMI6000 microscope utilizing a 100× 1.4 NA (O, STED) objective and two HyD detectors. Acquisitions were driven by a Leica motorized XY stage and Leica SuperZ Galvo with Adaptive Focus Control. Acquisition settings were controlled using the Leica LAS, Lightning Module software, with matched settings within experiments.

QUANTIFICATION AND STATISTICAL ANALYSIS

Image Analysis—Images acquired using Volocity or Leica LAS were analyzed directly with Volocity or exported as TIFF files and imported into the open-source software Fiji – ImageJ or Icy for analysis.

Quantifying total F-actin—Maximum intensity projections were exported from Volocity and analyzed in Fiji – ImageJ. A binary mask encompassing each individual cell was generated. The integrated F-actin intensity was measured within the mask and the integrated non-cellular background fluorescence was subtracted. For normalization, the average intensity per cell of control datasets were arbitrarily set to a value of 1, and individual cell measurements within each trial were expressed as the ratio of $Intensity_{Experimental\ cell}/Intensity_{Control\ cell}$.

Quantifying intracellular F-actin puncta—A single confocal section taken from the equator to bottom 1/3 of individual cells was analyzed in Volocity. A fluorescence intensity threshold generated by Otsu's method from maximum intensity projections was applied to single confocal sections and local intensity maxima were identified in 2D using the 'find spots' tool. Spots were restricted to a manually generated cytosolic ROI and a 0.4 mm radius was applied per spot to restrict over-sampling. Minimum spot intensities were offset by 1.5- and 1.85-fold that determined by Otsu's method for RAW264.7 and BMDM, respectively. Data are presented as cytosolic F-actin puncta identified per individual X-Y slice within a single cell.

Quantifying ASC foci—Maximum intensity projections acquired at 25× magnification were analyzed directly in Volocity software by the 'find objects' tool. ASC foci were defined by both a size threshold > 1 μm^3 and a fluorescence intensity threshold. Data were presented per number of nuclei analyzed.

F-actin Rab-association and BcCV fusion—Spinning disc confocal micrographs of infected macrophages were visually scored for the localization of Rab GTPases to cytosolic F-actin puncta and expressed as the percentage with positive Rab recruitment. To examine the accessibility of BcCVs to dextranloaded lysosomes, individual vacuoles were visually counted for dextran fluorescence and expressed as the percentage of dextranpositive BcCV.

Molecular coupling analysis—Confocal micrographs were exported from Volocity and single cell cropped composites comprising F-actin and WASH channels were generated in Fiji – ImageJ before importing into Icy software. Composites were analyzed using the SODA 2 color protocol in Icy (Lagache et al., 2018). Both F-actin and WASH spots were identified by the Wavelet Spot Detector Block (Scale 2) within a binary cell mask. Results and ROI statistics for single and coupled spots within individual cells were exported as xls files, and Mean Coupling Probability as well as *p-values* were extracted from 'SODAResults'.

Statistical analysis and graphs—Statistical comparison of the data was performed and plotted using GraphPad Prism 5. Sample size (total number of cells analyzed), the number of independent trials, dispersion and precision measures, and information on how significance was defined is found within individual Figure Legends. *P values* were determined by the two-tailed Mann-Whitney test between populations of individual cell measurements (Figures 1, 3, and 4). Statistical testing to generate a p value from Statistical Object Distance Analysis (Figure 2) is described elsewhere (Lagache et al., 2018) but assesses whether objects are randomly distributed (null hypothesis) and if objects couple significantly within a given analysis ring. Unpaired two-tailed Student's t test (Figures S3B and S3C), two-way ANOVA with Bonferroni post-test (Figures 5E, 5F, and S5G), and one-way ANOVA with Bonferroni's multiple comparison test (Figure S5C) were otherwise used to compare sets of matched samples. Data were not excluded from quantification, statistical analyses, or graphical representation. For each measurement, at least three independent experiments were performed.

Supplementary Material

Refer to Web version on PubMed Central for supplementary material.

ACKNOWLEDGMENTS

We thank Dr. Feng Shao (National Institute of Biological Sciences, Beijing, China) for providing isogenic *B. cenocepacia* WT and DtecA J2315 strains. G.F.W.W. is supported by a Vanier Canada Graduate Scholarship from the Canadian Institutes of Health Research (CIHR) and an MD/PhD Studentship from the University of Toronto. D.D.B. is supported by NIH grant R01DK107733. S.D.C. is supported by NIH R01HL088256 and R01AR070837. S.G. is supported by CIHR grant FDN-143202.

REFERENCES

Arakawa Y, Cordeiro JV, Schleich S, Newsome TP, and Way M (2007). The release of vaccinia virus from infected cells requires RhoA-mDia modulation of cortical actin. Cell Host Microbe 1, 227–240. [PubMed: 18005701]

Aubert DF, Xu H, Yang J, Shi X, Gao W, Li L, Bisaro F, Chen S, Valvano MA, and Shao F (2016). A Burkholderia Type VI Effector Deamidates Rho GTPases to Activate the Pyrin Inflammasome and Trigger Inflammation. Cell Host Microbe 19, 664–674. [PubMed: 27133449]

Burns JL, Jonas M, Chi EY, Clark DK, Berger A, and Griffith A (1996). Invasion of respiratory epithelial cells by Burkholderia (Pseudomonas) cepacia. Infect. Immun 64, 4054–4059. [PubMed: 8926068]

de Chaumont F, Dallongeville S, Chenouard N, Hervé N, Pop S, Provoost T, Meas-Yedid V, Pankajakshan P, Lecomte T, Le Montagner Y, et al. (2012). Icy: an open bioimage informatics platform for extended reproducible research. Nat. Methods 9, 690–696. [PubMed: 22743774]

Derivery E, Sousa C, Gautier JJ, Lombard B, Loew D, and Gautreau A (2009). The Arp2/3 activator WASH controls the fission of endosomes through a large multiprotein complex. Dev. Cell 17, 712–723. [PubMed: 19922875]

Dong R, Saheki Y, Swarup S, Lucast L, Harper JW, and De Camilli P (2016). Endosome-ER Contacts Control Actin Nucleation and Retromer Function through VAP-Dependent Regulation of PI4P. Cell 166, 408–423. [PubMed: 27419871]

Feng Y, Press B, and Wandinger-Ness A (1995). Rab 7: An Important Regulator of Late Endocytic Membrane Traffic. J Cell Biol 131, 1435–1452. [PubMed: 8522602]

Flannagan RS, Jaumouillé V, Huynh KK, Plumb JD, Downey GP, Valvano MA, and Grinstein S (2012). Burkholderia cenocepacia disrupts host cell actin cytoskeleton by inactivating Rac and Cdc42. Cell. Microbiol 14, 239–254. [PubMed: 22023324]

Gomez TS, Gorman JA, de Narvajas AA, Koenig AO, and Billadeau DD (2012). Trafficking defects in WASH-knockout fibroblasts originate from collapsed endosomal and lysosomal networks. Mol. Biol. Cell 23, 3215–3228. [PubMed: 22718907]

Govan JRW, Brown PH, Maddison J, Doherty CJ, Nelson JW, Dodd M, Greening AP, and Webb AK (1993). Evidence for transmission of Pseudomonas cepacia by social contact in cystic fibrosis. Lancet 342, 15–19. [PubMed: 7686239]

Graham DB, Osborne DG, Piotrowski JT, Gomez TS, Gmyrek GB, Akilesh HM, Dani A, Billadeau DD, and Swat W (2014). Dendritic cells utilize the evolutionarily conserved WASH and retromer complexes to promote MHCII recycling and helper T cell priming. PLoS ONE 9, e98606. [PubMed: 24886983]

Hao YH, Doyle JM, Ramanathan S, Gomez TS, Jia D, Xu M, Chen ZJ, Billadeau DD, Rosen MK, and Potts PR (2013). Regulation of WASH-dependent actin polymerization and protein trafficking by ubiquitination. Cell 152, 1051–1064. [PubMed: 23452853]

Hao Y-H, Fountain MD Jr., Fon Tacer K, Xia F, Bi W, Kang S-HL, Patel A, Rosenfeld JA, Le Caignec C, Isidor B, et al. (2015). USP7 Acts as a Molecular Rheostat to Promote WASH-Dependent Endosomal Protein Recycling and Is Mutated in a Human Neurodevelopmental Disorder. Mol. Cell 59, 956–969. [PubMed: 26365382]

Higgs HN, and Pollard TD (2000). Activation by Cdc42 and PIP(2) of Wiskott-Aldrich syndrome protein (WASp) stimulates actin nucleation by Arp2/3 complex. J. Cell Biol 150, 1311–1320. [PubMed: 10995437]

Holt PG, Strickland DH, Wikström m ME, and Jahnsen FL (2008). Regulation of immunological homeostasis in the respiratory tract. Nat. Rev. Immunol 8, 142–152. [PubMed: 18204469]

Huynh KK, Plumb JD, Downey GP, Valvano MA, and Grinstein S (2010). Inactivation of macrophage Rab7 by Burkholderia cenocepacia. J. Innate Immun 2, 522–533. [PubMed: 20829607]

Isles A, Maclusky I, Corey M, Gold R, Prober C, Fleming P, and Levison H (1984). Pseudomonas cepacia infection in cystic fibrosis: an emerging problem. J. Pediatr 104, 206–210. [PubMed: 6420530]

Jank T, and Aktories K (2008). Structure and mode of action of clostridial glucosylating toxins: the ABCD model. Trends Microbiol. 16, 222–229. [PubMed: 18394902]

Jia D, Gomez TS, Metlagel Z, Umetani J, Otwinowski Z, Rosen MK, and Billadeau DD (2010). WASH and WAVE actin regulators of the Wiskott-Aldrich syndrome protein (WASP) family are controlled by analogous structurally related complexes. Proc. Natl. Acad. Sci. USA 107, 10442–10447. [PubMed: 20498093]

Jia D, Gomez TS, Billadeau DD, and Rosen MK (2012). Multiple repeat elements within the FAM21 tail link the WASH actin regulatory complex to the retromer. Mol. Biol. Cell 23, 2352–2361. [PubMed: 22513087]

Johnson DE, Ostrowski P, Jaumouille V, and Grinstein S (2016). The position of lysosomes within the cell determines their luminal pH. J. Cell Biol 212, 677–692. [PubMed: 26975849]

Johnston RB Jr. (2001). Clinical aspects of chronic granulomatous disease. Curr. Opin. Hematol 8, 17–22. [PubMed: 11138621]

Keith KE, and Valvano MA (2007). Characterization of SodC, a periplasmic superoxide dismutase from Burkholderia cenocepacia. Infect. Immun 75, 2451–2460. [PubMed: 17325048]

Keith KE, Hynes DW, Sholdice JE, and Valvano MA (2009). Delayed association of the NADPH oxidase complex with macrophage vacuoles containing the opportunistic pathogen Burkholderia cenocepacia. Microbiology 155, 1004–1015. [PubMed: 19332803]

Lagache T, Grassart A, Dallongeville S, Faklaris O, Sauvonnet N, Dufour A, Danglot L, and Olivo-Marin J-C (2018). Mapping molecular assemblies with fluorescence microscopy and object-based spatial statistics. Nat. Commun 9, 698. [PubMed: 29449608]

Lamothe J, Huynh KK, Grinstein S, and Valvano MA (2007). Intracellular survival of Burkholderia cenocepacia in macrophages is associated with a delay in the maturation of bacteria-containing vacuoles. Cell. Microbiol 9, 40–53. [PubMed: 16869828]

MacDonald E, Brown L, Selvais A, Liu H, Waring T, Newman D, Bithell J, Grimes D, Urbe S, Clague MJ, and Zech T (2018). HRS-WASH axis governs actin-mediated endosomal recycling and cell invasion. J. Cell Biol 217, 2549–2564. [PubMed: 29891722]

Maloney KE, and Valvano MA (2006). The mgtC gene of Burkholderia cenocepacia is required for growth under magnesium limitation conditions and intracellular survival in macrophages. Infect. Immun 74, 5477–5486. [PubMed: 16988222]

Mansfield E, Chae JJ, Komarow HD, Brotz TM, Frucht DM, Aksentijevich I, and Kastner DL (2001). The familial Mediterranean fever protein, pyrin, associates with microtubules and colocalizes with actin filaments. Blood 98, 851–859. [PubMed: 11468188]

Masumoto J, Taniguchi S, Ayukawa K, Sarvotham H, Kishino T, Niikawa N, Hidaka E, Katsuyama T, Higuchi T, and Sagara J (1999). ASC, a novel 22-kDa protein, aggregates during apoptosis of human promyelocytic leukemia HL-60 cells. J. Biol. Chem 274, 33835–33838. [PubMed: 10567338]

McNally KE, Faulkner R, Steinberg F, Gallon M, Ghai R, Pim D, Langton P, Pearson N, Danson CM, Nä gele H, et al. (2017). Retriever is a multiprotein complex for retromer-independent endosomal cargo recycling. Nat. Cell Biol 19, 1214–1225. [PubMed: 28892079]

Nolen BJ, Tomasevic N, Russell A, Pierce DW, Jia Z, McCormick CD, Hartman J, Sakowicz R, and Pollard TD (2009). Characterization of two classes of small molecule inhibitors of Arp2/3 complex. Nature 460, 1031–1034. [PubMed: 19648907]

Phillips-Krawczak CA, Singla A, Starokadomskyy P, Deng Z, Osborne DG, Li H, Dick CJ, Gomez TS, Koenecke M, Zhang J-S, et al. (2015). COMMD1 is linked to the WASH complex and regulates endosomal trafficking of the copper transporter ATP7A. Mol. Biol. Cell 26, 91–103. [PubMed: 25355947]

Pollard TD, and Cooper JA (2009). Actin, a central player in cell shape and movement. Science 326, 1208–1212. [PubMed: 19965462]

Puthenveedu MA, Lauffer B, Temkin P, Vistein R, Carlton P, Thorn K, Taunton J, Weiner OD, Parton RG, and von Zastrow M (2010). Sequence-dependent sorting of recycling proteins by actin-stabilized endosomal microdomains. Cell 143, 761–773. [PubMed: 21111236]

Rizvi SA, Neidt EM, Cui J, Feiger Z, Skau CT, Gardel ML, Kozmin SA, and Kovar DR (2009). Identification and characterization of a small molecule inhibitor of formin-mediated actin assembly. Chem. Biol 16, 1158–1168. [PubMed: 19942139]

Rojas R, van Vlijmen T, Mardones GA, Prabhu Y, Rojas AL, Mohammed S, Heck AJR, Raposo G, van der Sluijs P, and Bonifacino JS (2008). Regulation of retromer recruitment to endosomes by sequential action of Rab5 and Rab7. J. Cell Biol 183, 513–526. [PubMed: 18981234]

Rosales-Reyes R, Skeldon AM, Aubert DF, and Valvano MA (2012). The Type VI secretion system of Burkholderia cenocepacia affects multiple Rho family GTPases disrupting the actin cytoskeleton

and the assembly of NADPH oxidase complex in macrophages. Cell. Microbiol 14, 255–273. [PubMed: 22023353]

Rotty JD, Wu C, Haynes EM, Suarez C, Winkelman JD, Johnson HE, Haugh JM, Kovar DR, and Bear JE (2015). Profilin-1 serves as a gatekeeper for actin assembly by Arp2/3-dependent and -independent pathways. Dev. Cell 32, 54–67. [PubMed: 25543281]

Saini LS, Galsworthy SB, John MA, and Valvano MA (1999). Intracellular survival of Burkholderia cepacia complex isolates in the presence of macrophage cell activation. Microbiology 145, 3465–3475. [PubMed: 10627044]

Sajjan U, Corey M, Humar A, Tullis E, Cutz E, Ackerley C, and Forstner J (2001). Immunolocalisation of Burkholderia cepacia in the lungs of cystic fibrosis patients. J. Med. Microbiol 50, 535–546. [PubMed: 11393291]

Sajjan US, Yang JH, Hershenson MB, and LiPuma JJ (2006). Intracellular trafficking and replication of Burkholderia cenocepacia in human cystic fibrosis airway epithelial cells. Cell. Microbiol 8, 1456–1466. [PubMed: 16922864]

Schindelin J, Arganda-Carreras I, Frise E, Kaynig V, Longair M, Pietzsch T, Preibisch S, Rueden C, Saalfeld S, Schmid B, et al. (2012). Fiji: an open-source platform for biological-image analysis. Nat. Methods 9, 676–682. [PubMed: 22743772]

Scoffone VC, Chiarelli LR, Trespidi G, Mentasti M, Riccardi G, and Buroni S (2017). Burkholderia cenocepacia Infections in Cystic Fibrosis Patients: Drug Resistance and Therapeutic Approaches. Front. Microbiol 8, 1592. [PubMed: 28878751]

Seaman MNJ, Harbour ME, Tattersall D, Read E, and Bright N (2009). Membrane recruitment of the cargo-selective retromer subcomplex is catalysed by the small GTPase Rab7 and inhibited by the Rab-GAP TBC1D5. J. Cell Sci 122, 2371–2382. [PubMed: 19531583]

Seaman MNJ, Gautreau A, and Billadeau DD (2013). Retromer-mediated endosomal protein sorting: all WASHed up!. Trends Cell Biol. 23, 522–528. [PubMed: 23721880]

Simonetti B, and Cullen PJ (2019). Actin-dependent endosomal receptor recycling. Curr. Opin. Cell Biol 56, 22–33. [PubMed: 30227382]

Suarez C, and Kovar DR (2016). Internetwork competition for monomers governs actin cytoskeleton organization. Nat. Rev. Mol. Cell Biol 17, 799–810. [PubMed: 27625321]

Suarez C, Carroll RT, Burke TA, Christensen JR, Bestul AJ, Sees JA, James ML, Sirotkin V, and Kovar DR (2015). Profilin regulates F-actin network homeostasis by favoring formin over Arp2/3 complex. Dev. Cell 32, 43–53. [PubMed: 25543282]

Takenawa T, and Suetsugu S (2007). The WASP-WAVE protein network: connecting the membrane to the cytoskeleton. Nat. Rev. Mol. Cell Biol 8, 37–48. [PubMed: 17183359]

Tsarouhas V, Liu D, Tsikala G, Fedoseienko A, Zinn K, Matsuda R, Billadeau DD, and Samakovlis C (2019). WASH phosphorylation balances endosomal versus cortical actin network integrities during epithelial morphogenesis. Nat. Commun 10, 2193. [PubMed: 31097705]

Villanueva J, Torregrosa-Hetland CJ, García-Martínez V, del Mar Francé s M, Viniegra S, and Gutié rrez LM (2012). The F-actin cortex in chromaffin granule dynamics and fusion: a minireview. J. Mol. Neurosci. 48, 323–327. [PubMed: 22350991]

Waite AL, Schaner P, Hu C, Richards N, Balci-Peynircioglu B, Hong A, Fox M, and Gumucio DL (2009). Pyrin and ASC co-localize to cellular sites that are rich in polymerizing actin. Exp. Biol. Med. (Maywood) 234, 40–52. [PubMed: 19109554]

Wang J, Fedoseienko A, Chen B, Burstein E, Jia D, and Billadeau DD (2018). Endosomal receptor trafficking: Retromer and beyond. Traffic 19, 578–590. [PubMed: 29667289]

Xu H, Yang J, Gao W, Li L, Li P, Zhang L, Gong YN, Peng X, Xi JJ, Chen S, et al. (2014). Innate immune sensing of bacterial modifications of Rho GTPases by the Pyrin inflammasome. Nature 513, 237–241. [PubMed: 24919149]

Zhang J, Shehabeldin A, da Cruz LA, Butler J, Somani AK, McGavin M, Kozieradzki I, dos Santos AO, Nagy A, Grinstein S, et al. (1999). Antigen receptor-induced activation and cytoskeletal rearrangement are impaired in Wiskott-Aldrich syndrome protein-deficient lymphocytes. J. Exp.Med 190, 1329–1342. [PubMed: 10544204]

Highlights

- *Burkholderia cenocepacia* induces formation of F-actin clusters in infected macrophages
- WASH is responsible for *de novo* F-actin polymerization near the phagosome
- WASH-dependent actin polymerization is induced by Rho GTPase inhibition
- Clustering of F-actin near phagosomes delays/prevents their maturation

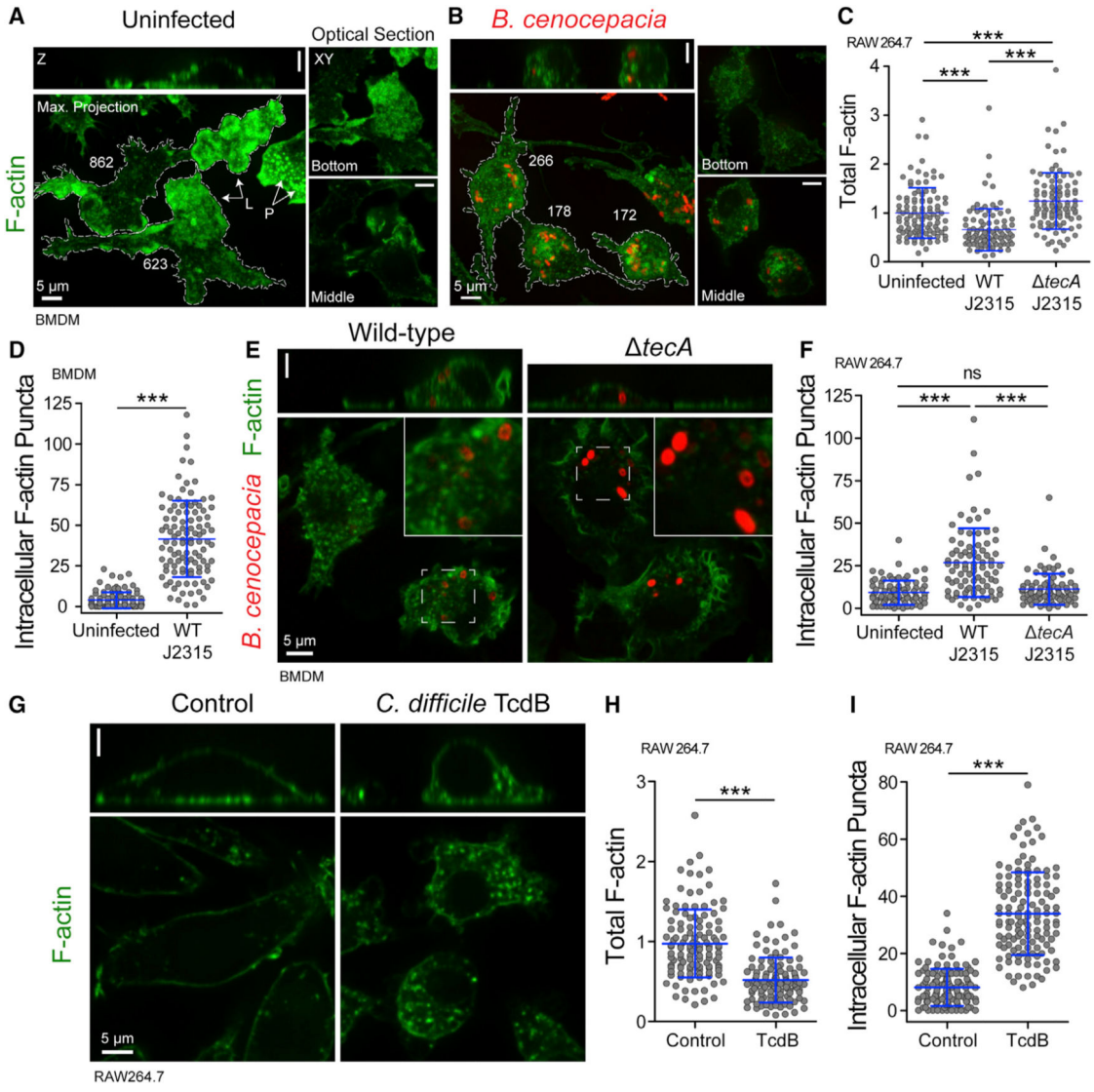

Figure 1. Inactivation of Rho GTPases by *B. cenocepacia* Induces Formation of F-actin Puncta in Macrophages

(A and B) Confocal micrographs of phalloidin-stained F-actin (green) in (A) uninfected BMDMs or (B) BMDMs infected for 2 h by opsonized monomeric red fluorescent protein 1 (RFP)-expressing WT J2315 (red, MOI 5). Maximum intensity projections (main panel), x-y slices (right panels), and corresponding x-z reconstructed views (top panel) are presented. Integrated F-actin values per cell shown (value 3 10^6 arbitrary fluorescence units, white dashed border). L, lamellipodium; P, podosomes. See also Videos S1 and S2.

(C) Comparison of normalized total F-actin content of uninfected or infected RAW264.7 cells. Data are individual cell measurements (gray, n > 100) and mean ± SD (blue) from 3 independent trials. Corresponding images in Figure S1C.

(D) Quantification of intracellular F-actin puncta from single confocal x-y sections in uninfected or WT J2315-infected BMDMs. Data are individual cell measurements (gray, n > 100) and mean ± SD (blue) from 3 independent trials.

(E) F-actin was stained (green) in BMDMs infected with fluorescently labeled WT or *ΔtecA* J2315 (red) for 2 h. Confocal micrographs representative of 3 experiments. Insets are enlarged from the indicated dashed boxes.
(F) Intracellular F-actin puncta quantified from single confocal sections of unifected RAW264.7 cells or cells infected with J2315 (WT or *ΔtecA*, MOI 10–20). Data are individual cell measurements (gray, n > 85) and mean ± SD (blue) from 3 independent trials. ns, not significantly different.
(G) F-actin was stained (green) in RAW264.7 cells left untreated (left) or treated with *C. difficile* TcdB for 2 h (right). Representative confocal sections acquired near the middle of the cell (bottom panels) and corresponding x-z views (top panels) shown.
(H) Normalized total F-actin content of individual control or TcdB-treated RAW264.7 cells were compared. Data are individual cell measurements (gray, n > 120) and mean ± SD (blue) from 3 independent trials.
(I) Intracellular F-actin puncta quantified from single confocal slices of control or TcdB-treated RAW264.7 cells. Data are individual cell measurements (gray, n > 100) and mean ± SD (blue) from 3 trials.
***p < 0.0001.

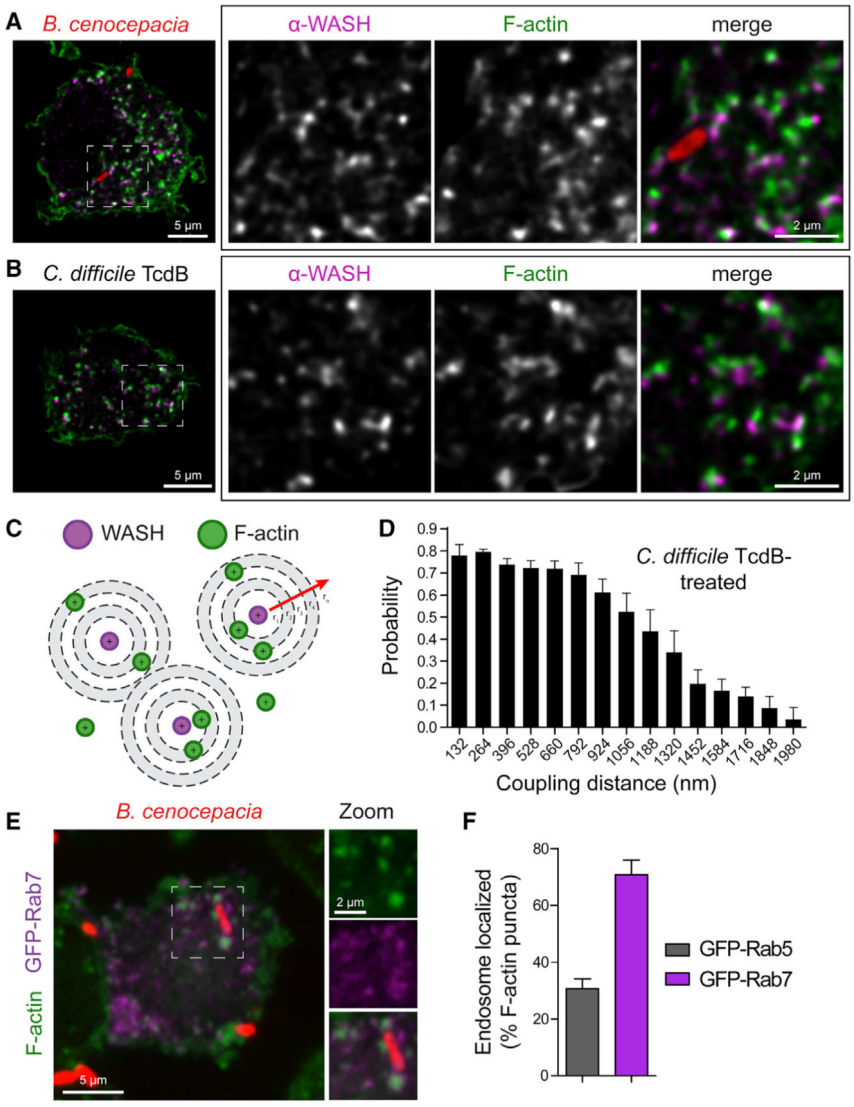

Figure 2. Intracellular F-actin Puncta that Form in Response to Inactivation of Rho GTPases Are Coupled to WASH

(A and B) Lightning microscopy of BMDMs infected with opsonized RFP-expressing J2315 (red) (A) or treated with TcdB (B) for 2 h followed by F-actin staining with phalloidin (green) and immunostaining of WASH (magenta). Inset: single and merged magnification of dotted white boxes. See also Videos S3 and S4.

(C) Model of 2D spatial coupling analysis between channel 1 (WASH) and channel 2 (F-actin) by SODA. Fluorescently labeled spots from each channel are first detected, and the localization of the center of intensity of each spot is specified by a marked point process. SODA uses the Ripley's K function combined with statistical thresholding relative to a random distribution (null hypothesis) to quantify the coupling probability of channel 2 spots in sequential concentric rings around channel 1 spots.

(D) SODA coupling analysis between WASH and F-actin by confocal microscopy (9 cells; 441 WASH spots, 476 F-actin spots). BMDMs were treated with TcdB for 2 h before

staining of WASH and F-actin. Association in the area defined by rings (r_1–r_4) is significant, with $p < 0.00001$ for all cells analyzed.

(E) Representative confocal section of a GFP-Rab7expressing RAW264.7 (magenta) infected with WT J2315 pJRL1 (red) for 2 h and F-actin stained (green). Insets are magnifications of dotted white boxes.

(F) F-actin puncta formed in transfected and infected cells from (E) were scored for localization to GFP-Rab5- or GFP-Rab7-positive endosomes. The percentage of puncta localizing to the endosomal population is presented as means ± SEM from 4 independent trials.

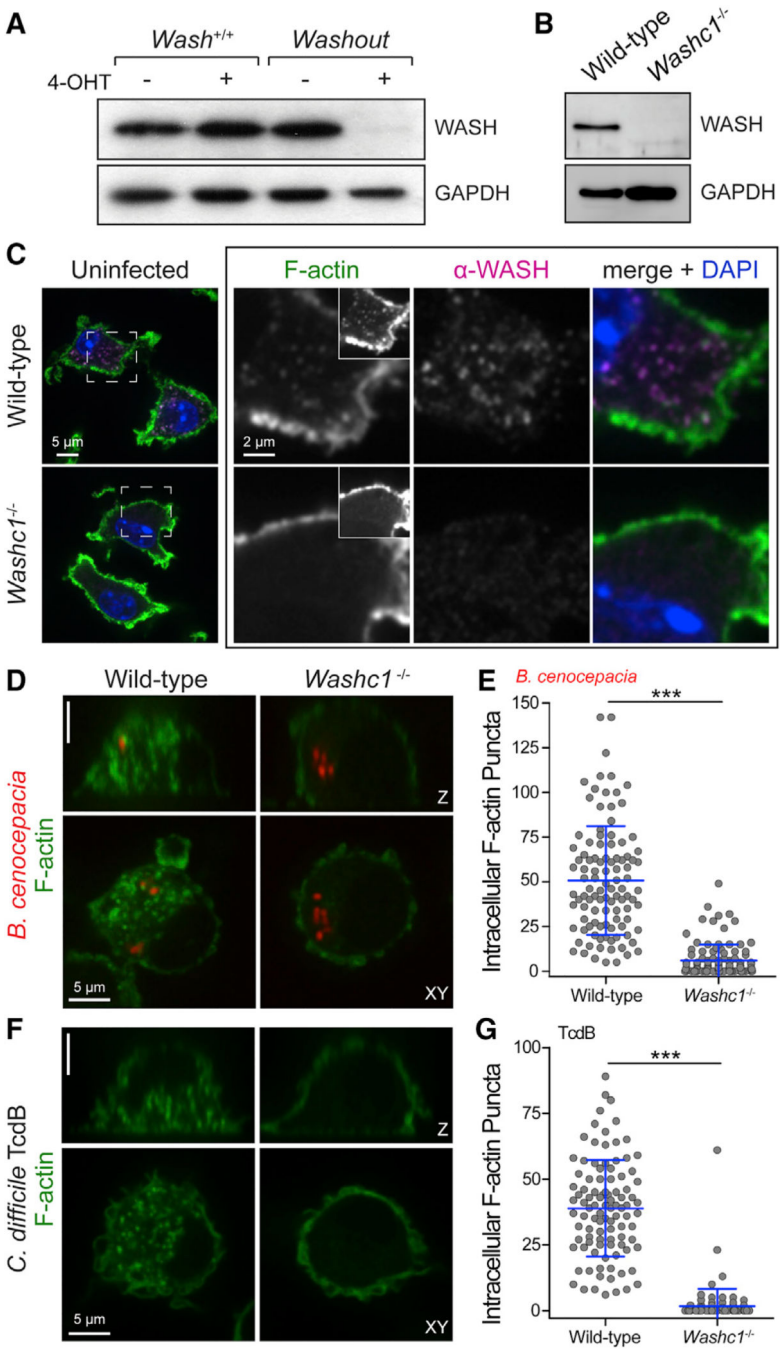

Figure 3. F-actin Puncta that Form in Response to B. cenocepacia Infection and TcdB Are WASH Dependent

(A) Expression of WASH in *Washc1*$^{flox/flox}$ (*Wash*$^{+/+}$) and *Washc1*$^{flox/flox}$/ERCre^{+} (*Washout*) assessed by immunoblotting in untreated (−) or 4-hydroxytamoxifen-treated (+) BMDMs.

(B) Expression of WASH in WT C57BL/6 and *Vav1*-Cre^{+}/*Washc1*$^{fl/fl}$ (*Washc1*$^{-/-}$) BMDMs evaluated by immunoblotting.

(C) Representative confocal section of F-actin staining (green), DAPI-stainednuclei (blue), and immunostained WASH (magenta) in uninfected WT (top panels) and *Washc1*$^{-/-}$ (bottom

panels) BMDMs. Magnifications of areas in dotted boxes are provided. Micrographs were acquired at equal laser power and exposure, but F-actin images were overexposed (2×) to reveal intracellular staining in insets.

(D) WT or *Washc1*$^{-/-}$ BMDMs were infected with opsonized WT J2315 (pJRL1, MOI 10, red) for 2 h before staining of F-actin (green). Confocal x-y slices (bottom panel) and corresponding z views (top panel).

(E) Quantification of intracellular F-actin puncta from single confocal sectionsin (D). Data are individual cell measurements (gray, n > 100) and mean ± SD (blue) from 3 independent experiments, each from 2 combined animals.

(F) WT or *Washc1*$^{-/-}$ BMDMs were treated with TcdB for 2 h before staining of F-actin (green). Confocal x-y slices (bottom panel) and corresponding z views (top panel).

(G) Quantification of intracellular F-actin puncta from single confocal sections in(F). Data are individual cell measurements (gray, n > 100) and mean ± SD (blue) from 3 independent experiments, each from 2 combined animals. ***p < 0.0001.

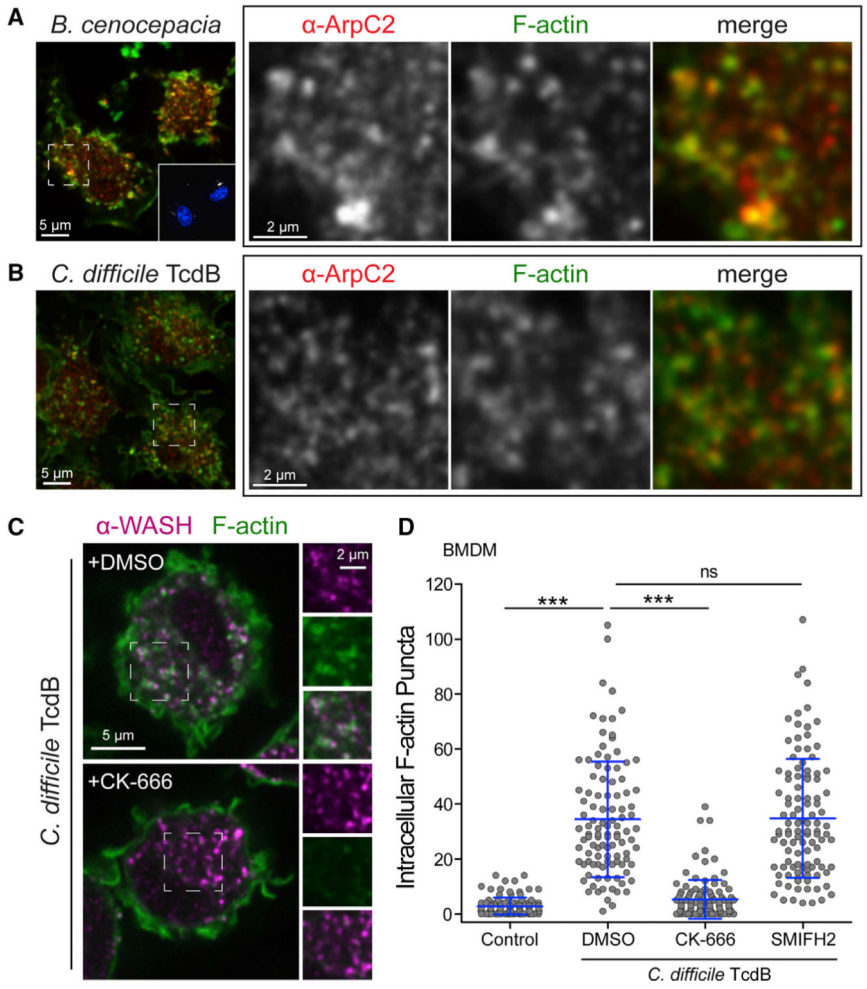

Figure 4. Formation of Intracellular F-actin Puncta Requires Actin Polymerization Driven by Arp2/3

(A and B) WT BMDMs were (A) infected with DyLight650-labeled WT J2315 (MOI 5, gray within inset) for 2 h or (B) treated with TcdB for 2 h before staining of ArpC2 (red) and F-actin (green). Magnified confocal micrographs of single and merged channels from areas contained within dotted white boxes are provided. See also Figure S4.

(C) After pre-incubation with TcdB, cells were incubated with Arp2/3 inhibitor (50 μM CK-666), Formin inhibitor (5 μM SMIFH2), or vehicle (DMSO) for 2 h. F-actin (green) and WASH were stained (magenta). Insets are enlarged from the indicated dashed white boxes.

(D) Intracellular F-actin puncta from (C) were quantified from single confocal slices. Mean ± SD (blue) is presented from individual cell measurements (gray, n > 100) from 3 experiments. ***p < 0.0001.

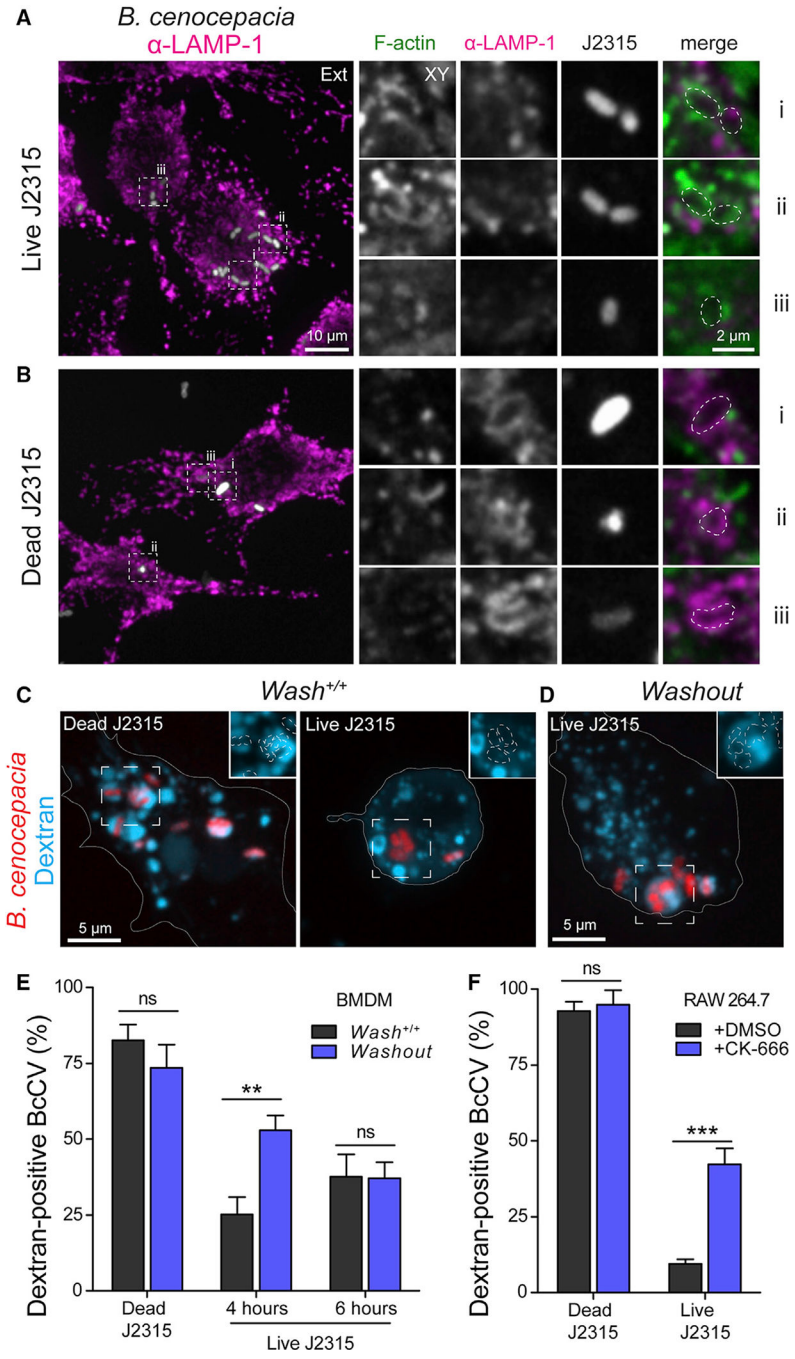

Figure 5. WASH and Arp2/3-Mediated Actin Polymerization Promote *B. Cenocepacia*-Induced Delay of Phagosome Maturation

(A and B) Live (A) or dead (B) opsonized J2315 (MOI 10 for 2 h, gray) were internalized by WT BMDMs before staining of LAMP-1 (magenta) and F-actin (green). Maximum intensity projections show the total distribution of LAMP-1 in infected cells (left panels). Right panel insets are magnifications of single confocal slices of white boxed regions around representative BcCV.

(C and D) Representative confocal micrographs of live or dead WT J2315 (pJRL1, red) internalized by (C) WT (*Wash*$^{+/+}$) or (D) Washout BMDMs. Confocal sections are presented

to encompass the entire BcCV and show distinct positioning or fusion of BcCV with dextran-loaded lysosomes (cyan). The positions of individual bacteria are indicated by dotted lines.

(E) Percentage of dextran-positive BcCV, indicatingfusion with lysosomes, quantified in infected cells from (C) and (D). Data are means ± SEM from at least 3 experiments. **$p < 0.01$.

(F) Percentage of dextran-positive BcCV quantifiedin RAW264.7 cells infected with live or dead WT J2315 (pJRL1) and treated with vehicle (DMSO) or Arp2/3 inhibitor (CK-666) until 2 h post-infection. Data are means ± SEM from 3 independent trials ($n > 70$ infected cells per condition). ***$p < 0.001$.

KEY RESOURCES TABLE

REAGENT or RESOURCE	SOURCE	IDENTIFIER
Antibodies		
anti-LAMP1 (rat, clone 1D4B)	Developmental Studies Hybridoma Bank	Cat#1D4B; RRID: AB_2134500
anti-p34-Arc/ARPC2 (rabbit)	EMD Millipore	Cat#07-227; RRID: AB_310447
anti-WASH (rabbit, against mouse VCA domain)	Gomez et al., 2012	Cat#Billadeau_mWASH; RRID: AB_2848164
anti-ASC (mouse, clone HASC-71)	BioLegend	Cat#653902; RRID: AB_2561778
anti-Caspase-1 (rabbit)	Santa Cruz	Cat#sc-514; RRID: AB_2068895
anti-GAPDH (mouse, clone 6C5)	EMD Millipore	Cat#MAB374; RRID: AB_2107445
Donkey anti-mouse, anti-rabbit, or anti-rat (Cy3- or Alexa Fluor 647-conjugated)	Jackson ImmunoResearch	Cat#715-605-151; RRID:AB_2340863, #711-605-152; RRID:AB_2492288, #711-165-152; RRID:AB_2307443, #712-605-153; RRID:AB_2340694
Bacterial and Virus Strains		
B. cenocepacia J2315 (WT pJRL1, with monomeric red fluorescent protein 1 (RFP)	Lamothe et al., 2007	N/A
B. cenocepacia J2315 (WT)	Aubert et al., 2016	N/A
B. cenocepacia J2315 (Δ*tecA*)	Aubert et al., 2016	N/A
Chemicals, Peptides, and Recombinant Proteins		
FuGENE HD	Promega Corporation	Cat#E2311
LB Broth Miller	BioShop	Cat#LBL407.5
Carbenicillin Disodium	Wisent Bio Products	Cat#400-112-IG
Trimethoprim	Sigma-Aldrich	Cat#T7883
Amersham ECL Prime Western Blotting Detection Reagent	GE Healthcare	Cat#RPN2232
Phosphate-buffered Saline (PBS)	Wisent Bio Products	Cat#311-010-CL
CK-666	Calbiochem	Cat#182515
Dimethyl sulfoxide (DMSO)	Sigma-Aldrich	Cat#D2650
Paraformaldehyde (PFA)	Electron Microscopy Sciences	Cat#15710
C. difficile Toxin B (TcdB)	List Biological Laboratories	Cat#155A
SMIFH2	Calbiochem	Cat#344092
Alexa Fluor 488 phalloidin	Thermo Fisher Scientific	Cat#A12379
4′,6-diamidino-2-phenylindole dihydrochloride (DAPI)	Thermo Fisher Scientific	Cat. #D1306
Dextran, Alexa Fluor 647; 10,000 MW, Anionic, Fixable	Thermo Fisher Scientific	Cat#D22914
(Z)-4-Hydroxytamoxifen	Sigma-Aldrich	Cat#H7904
Recombinant Murine M-CSF	PeproTech Inc.	Cat#315-02
Albumin	BioShop	Cat#ALB001
Saponin	Calbiochem	Cat#558255
Latrunculin A	Sigma-Aldrich	Cat#L5163
Triton X-100	Thermo Fisher Scientific	Cat#BP151-500
Goat Serum	Wisent Bio Products	Cat#053-150

REAGENT or RESOURCE	SOURCE	IDENTIFIER
DyLight 650 NHS Ester	Thermo Fisher Scientific	Cat#62265
Alexa Fluor 568 NHS Ester	Thermo Fisher Scientific	Cat#A20003
Filtered human serum (male and female)	University of Toronto	N/A
Trichloroacetic acid (TCA)	Fisher Scientific	Cat#A322-500
Antibiotic-Antimycotic Solution	Wisent Bio Products	Cat#450-115-EL
Ethylenediaminetetraacetic acid (EDTA)	Thermo Fisher Scientific	Cat#SS412-1
Nigericin sodium salt	Sigma-Aldrich	Cat#N7143
Lipopolysaccharides (rough strains) from *Salmonella enterica* serotype minnesota	Sigma-Aldrich	Cat#L9764
Critical Commercial Assays		
Pierce LDH Cytotoxicity Assay Kit	Thermo Fisher Scientific	Cat#PI88954
HiSpeed Plasmid Maxi Kit	QIAGEN	Cat#12663
Experimental Models: Cell Lines		
Mouse: RAW 264.7 monocyte macrophages	ATCC	ATCC: TIB-71
Human: HeLa cells	ATCC	ATCC: CCL-2
Experimental Models: Organisms/Strains		
Mouse: C57BL/6 wildtype	The Jackson Laboratory	JAX: 000664
Mouse: *Washc1*$^{fl/fl}$	Gomez et al., 2012; Daniel D. Billadeau Laboratory	N/A
Mouse: ER-Cre^{+}/*Washc1*$^{fl/fl}$	Gomez et al., 2012; Daniel D. Billadeau Laboratory	N/A
Mouse: *Vav1*-Cre^{+}/*Washc1*$^{fl/fl}$	Graham et al., 2014; Sergio D. Catz and Daniel D. Billadeau Laboratories	N/A
Mouse: *WAS*$^{-/-}$	Zhang et al., 1999	N/A
Recombinant DNA		
GFP-Rab5	Provided by Dr. Craig Roy, Yale University, USA	N/A
GFP-Rab7	Provided by Dr. Angela Wandinger-Ness, University of New Mexico Health Sciences Center, USA – see Feng et al., 1995	N/A
Software and Algorithms		
Volocity	PerkinElmer Inc.	https://www.perkinelmer.com/lab-products-and-services/product-support.html#Volocity
Fiji – ImageJ	Schindelin et al., 2012	https://imagej.net/Fiji
Icy	de Chaumont et al., 2012	http://icy.bioimageanalysis.org/
GraphPad Prism 5	GraphPad Software	https://www.graphpad.com/scientific-software/prism/